Prompt fission neutron emission in neutron and proton induced reactions at intermediate energies

V. A. Rubchenya*
Department of Physics, University of Jyväskylä, FIN-40014, Jyväskylä, Finland and
V. G. Khlopin Radium Institute, RU-194021 St. Petersburg, Russia
(Received 18 December 2006; published 2 May 2007)

The generalized model for the description of the prompt fission neutron spectra and multiplicities at neutron and proton energies up to about 100 MeV is described. The three main emission mechanisms considered are the precompound emission, the pre-scission particle evaporation before the saddle point and at descent to the scission point, and the emission from excited fission fragments. The two-component exciton model is used for the description of the preequilibrium stage of the reaction. The time-dependent statistical model with inclusion of the nuclear friction effects describes particle evaporation starting just after the precompound emission stage and lasting for the duration of the evolution of the compound nucleus toward scission. The fragment mass distribution and fission fragment kinetic and excitation energies are determined from the properties of the composite system at the scission point. The particle spectra from the fission fragments are calculated within the statistical approach. These spectra are then transformed into the laboratory rest frame using the calculated fragment kinetic energies and are averaged over the calculated fragment mass distributions. The model was applied to analyze the prompt fission neutron characteristics in the proton and neutron induced fission of actinide nuclei, and comparisons with the experimental data in ^{238}U(n, f), ^{238}U(p, f), and ^{242}Pu(p, f) reactions are presented.

DOI: 10.1103/PhysRevC.75.054601 PACS number(s): 24.10.−i, 24.75.+i, 25.85.Ec, 25.85.Ge

I. INTRODUCTION

Prompt fission neutrons are widely used as time and temperature probes in the heavy ion fusion-fission and quasifission reactions [1]. Due to a larger velocity of the center-of-mass frame in the heavy ion reactions than in neutron and light-charged-particle induced reactions, the extraction of the pre- and post-scission component is more difficult in the last case. Therefore only a few experiments have been done to measure pre- and post-neutron multiplicities in the neutron and proton induced fission at intermediate energies [2–6]. At the projectile energy greater than 10 MeV, the contribution of the precompound emission plays an important role in removing the substantial part of the initial excitation energy. At present, information about spectra and multiplicities of neutrons emitted at the preequilibrium stage reaction is scarce [6]. The statistical part of the pre-scission neutrons is evaporated before passing the saddle point and during the descent from the saddle point to the scission where the dynamical effects of the nuclear friction may play an important role [1].

The properties of the post-scission neutrons are mainly formed as a result of evaporation from the fully accelerated heated fission fragments with some distributions of the kinetic and excitation energies. In the pioneering work of Ref. [7], the prompt neutron spectrum was described by the one-source model with a temperature parameter and averaged fission fragment kinetic energy. Then several versions of the multiple-source neutron emission statistical models of spontaneous and low-energy fission were proposed [8–12].

With increasing neutron or proton bombarding energy above the second and higher order fission thresholds, the pre-scission neutron spectra and contributions from different compound nuclei to the post-scission particle emission should be included into consideration. Recently two approaches for calculating the prompt neutron spectra in the neutron induced fission of ^{232}Th and ^{238}U at neutron energy below 20 MeV were proposed [13–15]. These works focused mainly on the accurate calculation of the different fission chance contributions to the fission cross section while treating the post-scission emission in the simplified way. The semiempirical extrapolation of the Los Alamos model [9] for the neutron induced fission of ^{238}U to the intermediate energy was used to calculate the prompt fission neutron multiplicity and spectra [16].

This paper presents the unified model approach for calculating the prompt fission neutron spectra and multiplicities in neutron and proton induced fission at projectile energies up to 100 MeV. Neutron emission may occur at any of the three stages of the reaction: (1) the fast preequilibrium process, (2) the time when the collective fission degree of freedom builds up and the compound nucleus passes to the scission point, and (3) the neutron evaporation from the heated fission fragments. The precompound neutron and proton emission process is described using the two-component exciton model. The initial excitation energy distribution of the compound nucleus is defined by the spectra and multiplicities of particles emitted at the preequilibrium stage. The decay of the compound nucleus is treated within the time-dependent statistical model with inclusion of nuclear friction effects in the calculation of the fission width and the descent time from the saddle to the scission point. The pre-scission neutron spectra and multiplicities are formed during the time interval between the end of the preequilibrium stage and when the scission point is reached. The composition and excitation energy distribution

*Electronic address: rubchen@phys.jyu.fi

of the compound nucleus at the scission point are defined by the neutron and proton multiplicities and energy elapsed at the preequilibrium stage and collective motion stage to the scission. The excitation and kinetic energies of the primary fission fragments are calculated in the framework of the fission scission point model with inclusion of the shell structure effects. The post-scission neutron spectra and multiplicities are calculated within the cascade emission model. The fission fragment yield integrated post-scission spectrum is obtained using the mass yield curve determined in the multimodal fission model.

The present study is devoted to the investigation of the dynamical interplay between the preequilibrium, statistical pre-scission, and post-scission prompt fission neutron emission mechanisms. Accurate calculation of neutron and proton emission is crucial for the estimation of the cross section formation of the extremely neutron-rich fission products. The model and calculation method developed in the present paper may be used for beam intensity predictions for the future radioactive ion beam facilities.

II. THEORETICAL MODEL

The prompt fission neutron double differential spectrum at the given projectile energy integrated over fragment mass and charge distributions can be presented in the form

$$\frac{d^2M_n}{dE_n d\Omega_n} = \frac{d^2M_n^{\text{preeq}}}{dE_n d\Omega_n} + \frac{d^2M_n^{\text{pre-sc}}}{dE_n d\Omega_n} + \frac{d^2M_n^{\text{post-sc}}}{dE_n d\Omega_n}, \qquad (1)$$

where E_n is the neutron energy in the laboratory frame and M_n is the average neutron multiplicity formed by the neutron emission at the preequilibrium, pre-scission, and post-scission stages of the fission process. In the reaction between the target with spin I and the projectile with spin s, the partial composite nucleus formation cross section is approximately equal to the partial reaction cross section and can be obtained from the optical model

$$\sigma_{ljIJ}^{CF}\left(A_{CF}, Z_{CF}, E_{\text{ex}}^{CF}\right) = \frac{\pi\bar{\lambda}^2}{2I+1}(2J+1)T_{lI}^{J}, \qquad (2)$$

where $A_{\text{CF}}, Z_{\text{CF}}$, and $E_{\text{ex}}^{\text{CF}}$ are initial mass and charge numbers and excitation energy of the composite nucleus, $\vec{J} = \vec{I} + \vec{j}$ and $\vec{j} = \vec{l} + \vec{s}$ are the channel and projectile spin, and T_{ljI}^{J} is the projectile transmission coefficients. For each partial entrance channel, there is some probability $P_{lJ}^{\text{preeq}}(\Delta N^{\text{preeq}}, \Delta Z^{\text{preeq}}, \Delta E_{\text{ex}}^{\text{preeq}}, \Delta J^{\text{preeq}})$ of the preequilibrium emission of ΔN^{preeq} neutrons and ΔZ^{preeq} protons, which remove excitation energy $\Delta E_{\text{ex}}^{\text{preeq}}$ and the angular momentum ΔJ^{preeq}. In this case, the partial compound nucleus formation cross section is defined by the expressions

$$\begin{aligned}
&\sigma_{ljIJ_{\text{CN}}}^{\text{CN}}\left(A_{\text{CN}}, Z_{\text{CN}}, E_{\text{ex}}^{\text{CN}}\right) \\
&\quad = \sigma_{ljIJ}^{\text{CF}} P_{lJ}^{\text{preeq}}\left(\Delta N^{\text{preeq}}, \Delta Z^{\text{preeq}}, \Delta E_{\text{ex}}^{\text{preeq}}, \Delta J^{\text{preeq}}\right), \\
&A_{\text{CN}} = A_{\text{CF}} - \Delta N^{\text{preeq}} - \Delta Z^{\text{preeq}}, \\
&Z_{\text{CN}} = Z_{\text{CF}} - \Delta Z^{\text{preeq}}, \\
&E_{\text{ex}}^{\text{CN}} = E_{\text{ex}}^{\text{CF}} - \Delta E_{\text{ex}}^{\text{preeq}}, \quad J_{\text{CN}} = J - \Delta J^{\text{preeq}}. \qquad (3)
\end{aligned}$$

The preequilibrium particle emission process is described in the frame of the two-component exciton model and will be considered in the next subsection.

After ending the preequilibrium stage for every partial wave in the entrance channel, consideration of the decay of compound nuclei states starts. It is supposed that the duration of the preequilibrium process is two orders of magnitude shorter than the average statistical decay time of the initial composite nucleus. Therefore, formation and deexcitation stages of the compound nuclei are decoupled. The pre-scission neutrons are emitted near the equilibrium deformation of the compound nucleus and at the descent from saddle to scission point. The emission time is strongly influenced by nuclear friction [1]. After pre-scission particle emission, the compound nucleus arrives at the scission point with some distribution of excitation energy $E_{\text{ex}}^{\text{sc}}$, mass $A_{\text{CN}}^{\text{sc}}$, charge $Z_{\text{CN}}^{\text{sc}}$ numbers, and spin J_{sc}.

The post-scission neutrons are evaporated from the fully accelerated excited primary fission fragments. For each primary fragment with mass A and charge Z, the average excitation and kinetic energies are calculated in the framework of the fission scission point model. The average post-scission neutron multiplicities and evaporated neutron spectra are calculated for each member of the fission fragment ensemble.

A. Precompound stage of reaction

At $E_{\text{proj}}/A_{\text{proj}} \geqslant 10$ MeV/u, the thermally equilibrated compound nuclei are formed after preequilibrium emission of neutrons, protons, and other light particles. But in the case of the heavy fissile nuclei, the probability of the light-charged-particle emission is very low compared to neutron and proton precompound emission because of the Coulomb barrier. Here we use a two-component exciton model [17,18] for our objective: adequate description of the initial excitation energy distribution and composition of the compound nuclei in the neutron and proton induced fission at the incident energy of 10 to 100 MeV.

The two-component exciton model considers time evolution of a nuclear reaction in terms of time-dependent population of exciton states, which are characterized by the proton (p_π) and neutron (p_ν) particle numbers and the proton (h_π) and neutron (h_ν) hole numbers. The exciton states are described by four numbers ($p_\pi, h_\pi, p_\nu, h_\nu$) with the proton exciton number $n_\pi = p_\pi + h_\pi$, the neutron exciton number $n_\nu = p_\nu + h_\nu$, and the exciton number $n = n_\pi + n_\nu$.

The initial states for the proton and neutron induced reactions are (1, 0, 0, 0) and (0, 0, 1, 0), respectively. From these initial states there is no particle emission because that process is included in the elastic scattering of the incident particles. Two-body interactions generate transitions to other states with selection rule $\Delta n = 0, 2$ neglecting the decay of exciton states into less complex states by pair annihilation.

That is known historically in the one-component model as the "never come back" approximation.

Starting from the second step of the exciton system evolution process, the following transitions from exciton state $(p_\pi, h_\pi, p_\nu, h_\nu)$ are taken into account:

(i) Proton particle-hole pair creation producing $(p_\pi + 1, h_\pi + 1, p_\nu, h_\nu)$ exciton states with the transition rate $\lambda_\pi^+(p_\pi, h_\pi, p_\nu, h_\nu)$.
(ii) Neutron particle-hole creation producing $(p_\pi, h_\pi, p_\nu + 1, h_\nu + 1)$ exciton states with the transition rate $\lambda_\nu^+(p_\pi, h_\pi, p_\nu, h_\nu)$.
(iii) The conversion of a proton particle-hole pair into a neutron particle-hole pair creation: transition from $(p_\pi, h_\pi, p_\nu, h_\nu)$ exciton states into $(p_\pi - 1, h_\pi - 1, p_\nu + 1, h_\nu + 1)$ with the transition rate $\lambda_{\pi\nu}^0(p_\pi, h_\pi, p_\nu, h_\nu)$.
(iv) The conversion of a neutron particle-hole pair into a proton particle-hole pair creation: transition from $(p_\pi, h_\pi, p_\nu, h_\nu)$ exciton states into $(p_\pi + 1, h_\pi + 1, p_\nu - 1, h_\nu - 1)$ with the transition rate $\lambda_{\nu\pi}^0(p_\pi, h_\pi, p_\nu, h_\nu)$.
(v) The proton emission producing the exciton states $(p_\pi - 1, h_\pi, p_\nu, h_\nu)$, $\Delta n = \Delta n_\pi = -1$ with the transition rate $\lambda_\pi^{\mathrm{em}}(p_\pi, h_\pi, p_\nu, h_\nu)$.
(vi) The neutron emission producing the exciton states $(p_\pi, h_\pi, p_\nu - 1, h_\nu)$, $\Delta n = \Delta n_\nu = -1$ with the transition rate $\lambda_\nu^{\mathrm{em}}(p_\pi, h_\pi, p_\nu, h_\nu)$.
(vii) After the neutron or proton emission, the exciton evolution process may develop further until reaching the criteria for transition to the equilibrium stage of the nuclear reaction. Thus the multiple-particle preequilibrium emission is included in the model.

The lifetime of exciton state $(p_\pi, h_\pi, p_\nu, h_\nu)$ at the excitation energy E_x is defined as the inverse sum of the various transition rates,

$$\tau(p_\pi, h_\pi, p_\nu, h_\nu) = \left[\lambda_\pi^+ + \lambda_\nu^+ + \lambda_{\pi\nu}^0 + \lambda_{\nu\pi}^0 + \lambda_\pi^{\mathrm{em}} + \lambda_\nu^{\mathrm{em}}\right]^{-1}. \quad (4)$$

In this study, the emission rates of complex particles are supposed to be negligible for the heavy composite nuclei.

The transition rates for the creation of new proton and neutron particle-hole pairs consist of four terms corresponding to p_π, h_π, p_ν, and h_ν scattering, which leads to new particle-hole pairs [18],

$$\lambda_\pi^+(p_\pi, h_\pi, p_\nu, h_\nu) = \frac{1}{\rho(p_\pi, h_\nu, p_\nu, h_\nu, E_x)} \frac{2\pi}{\hbar} \times \left[M_{\pi\pi}^2 \int_{U_1^{p\pi}}^{U_2^{p\pi}} \rho(2, 1, 0, 0, U)\rho(p_\pi - 1, h_\pi, p_\nu, h_\nu, E_x - U)\rho(1, 0, 0, 0, U)\, dU + M_{\pi\pi}^2 \int_{U_1^{h\pi}}^{U_2^{h\pi}} \rho(1, 2, 0, 0, U)\rho(p_\pi h_\pi - 1, p_\nu, h_\nu, E_x - U)\rho(0, 1, 0, 0, U)\, dU + M_{\nu\pi}^2 \int_{U_1^{p\nu}}^{U_2^{p\nu}} \rho(1, 1, 1, 0, U)\rho(p_\pi h_\pi, p_\nu - 1, h_\nu, E_x - U)\rho(0, 0, 1, 0, U)\, dU + M_{\nu\pi}^2 \int_{U_1^{h\nu}}^{U_2^{h\nu}} \rho(1, 1, 0, 1, U)\rho(p_\pi, h_\pi, p_\nu, h_\nu - 1, E_x - U)\rho(0, 0, 0, 1, U)\, dU \right]. \quad (5)$$

$$\lambda_\nu^+(p_\pi, h_\pi, p_\nu, h_\nu) = \frac{1}{\rho(p_\pi, h_\nu, p_\nu, h_\nu, E_x)} \frac{2\pi}{\hbar} \times \left[M_{\nu\nu}^2 \int_{U_1^{p\nu}}^{U_2^{p\nu}} \rho(0, 0, 2, 1, U)\rho(p_\pi, h_\pi, p_\nu - 1, h_\nu, E_x - U)\rho(0, 0, 1, 0, U)\, dU + M_{\nu\nu}^2 \int_{U_1^{h\nu}}^{U_2^{h\nu}} \rho(0, 0, 1, 2, U)\rho(p_\pi, h_\pi, p_\nu, h_\nu - 1, E_x - U)\rho(0, 0, 0, 1, U)\, dU + M_{\pi\nu}^2 \int_{U_1^{p\pi}}^{U_2^{p\pi}} \rho(1, 0, 1, 1, U)\rho(p_\pi - 1, h_\pi, p_\nu, h_\nu, E_x - U)\rho(1, 0, 0, 0, U)\, dU + M_{\pi\nu}^2 \int_{U_1^{h\pi}}^{U_2^{h\pi}} \rho(0, 1, 1, 1, U)\rho(p_\pi, h_\pi - 1, p_\nu, h_\nu, E_x - U)\rho(0, 1, 0, 0, U)\, dU \right]. \quad (6)$$

Here the first and third terms represent particle scattering, and the second and fourth terms represent hole scattering. The values $\rho(p_\pi, h_\pi, p_\nu, h_\nu, U)$ stand for the two-component particle-hole state density at the excitation energy U. The integration limits account for the corrections in the particle-hole state density formula for the Pauli exclusion principle (see Ref. [18]).The average squared matrix elements of the residual interaction in the proton-proton $M_{\pi\pi}^2$, neutron-neutron $M_{\nu\nu}^2$, proton-neutron $M_{\pi\nu}^2$, and neutron-proton $M_{\nu\pi}^2$ channels are assumed to depend only on the total excitation energy E_x of the whole composite nucleus. The two-component matrix elements are parametrized by M^2 and R:

$$\begin{aligned} M_{\pi\pi}^2 &= M_{\nu\nu}^2 = M^2, \\ M_{\pi\nu}^2 &= M_{\nu\pi}^2 = RM^2. \end{aligned} \quad (7)$$

In Ref. [18], the new parametrization for the squared matrix element was proposed as

$$M^2 = \frac{1}{A^3}\left[6.8 + \frac{4.2 \times 10^5}{\left(\frac{E_x}{n} + 10.7\right)^3}\right] \quad \text{and} \quad R = 1.5. \quad (8)$$

The transition rates for conversion of a proton or neutron particle-hole pair into a neutron or proton particle-hole pair

are

$$\lambda^0_{\pi\nu}(p_\pi, h_\pi, p_\nu, h_\nu) = \frac{1}{\rho(p_\pi, h_\nu, p_\nu, h_\nu, E_x)}\frac{2\pi}{\hbar} \times M^2_{\pi\nu}\int_{U_1^{p\nu}}^{U_2^{p\nu}} \rho(0,0,1,1,U)\rho(p_\pi - 1, h_\pi - 1, p_\nu, h_\nu, E_x - U)\rho(1,1,0,0,U)\,dU, \quad (9)$$

$$\lambda^0_{\nu\pi}(p_\pi, h_\pi, p_\nu, h_\nu) = \frac{1}{\rho(p_\pi, h_\nu, p_\nu, h_\nu, E_x)}\frac{2\pi}{\hbar} \times M^2_{\nu\pi}\int_{U_1^{p\nu}}^{U_2^{p\nu}} \rho(1,1,0,0,U)\rho(p_\pi, h_\pi, p_\nu - 1, h_\nu - 1, E_x - U)\rho(0,0,1,1,U)\,dU. \quad (10)$$

The formula for the particle-hole state density $\rho(p_\pi, h_\pi, p_\nu, h_\nu, U)$ is based on the assumption of equidistant single-particle level spacing and contains the pairing, the Pauli exclusion principle, and the potential well finite depth corrections [18]. The two-component particle-hole density is

$$\rho(p_\pi, h_\pi, p_\nu, h_\nu, E_x) = \frac{g_\pi^{n_\pi} g_\nu^{n_\nu}}{p_\pi! h_\pi! p_\nu! h_\nu! (n-1)!} \times (E_x - P_{p,h} - \varepsilon_P(p_\pi, h_\pi, p_\nu, h_\nu))^{n-1} f(p, h, E_x), \quad (11)$$

where E_x is total excitation energy, and g_π and g_ν are single-particle state densities. The pairing correction $P_{p,h}$ was calculated using parametrization from Ref. [19]. The parametrization of the Pauli exclusion principle correction term $\varepsilon_P(p_\pi, h_\pi, p_\nu, h_\nu)$ and the finite potential well depth correction function $f(p, h, E_x)$ can be found in Ref. [18]. For the single-particle state densities, approximations were used:

$$g_\pi = Z/15, \quad g_\nu = N/15\,\mathrm{MeV}^{-1}. \quad (12)$$

The proton and neutron single spectra emitted from a given exciton state are given by

$$\frac{dW^s_\pi(p_\pi, h_\pi, p_\nu, h_\nu, E_\pi)}{dE_\pi} = \frac{2\mu_\pi}{\pi^2\hbar^3} \times \frac{\rho(p_\pi - 1, h_\pi, p_\nu, h_\nu, E_x - B_\pi - E_\pi)}{\rho(p_\pi, h_\pi, p_\nu, h_\nu, E_x)}\sigma_\pi^{\mathrm{inv}}(E_\pi)E_\pi, \quad (13)$$

$$\frac{dW^s_\nu(p_\pi, h_\pi, p_\nu, h_\nu, E_\nu)}{dE_\nu} = \frac{2\mu_\nu}{\pi^2\hbar^3} \times \frac{\rho(p_\pi, h_\pi, p_\nu - 1, h_\nu, E_x - B_\nu - E_\nu)}{\rho(p_\pi, h_\pi, p_\nu, h_\nu, E_x)}\sigma_\nu^{\mathrm{inv}}(E_\nu)E_\nu, \quad (14)$$

Here $\mu_\pi, B_\pi, E_\pi, \sigma_\pi^{\mathrm{inv}}(E_\pi)$ are the proton reduced mass, proton binding energy, center-of-mass frame proton energy, and inverse reaction cross section, calculated with the optical model; and $\mu_\nu, B_\nu, E_\nu, \sigma_\nu^{\mathrm{inv}}(E_\nu)$ have the same meanings for neutrons. The corresponding emission rates $\lambda_\pi^{\mathrm{em}}, \lambda_\nu^{\mathrm{em}}$ can be obtained by integration over the emitted particle energy.

The Monte Carlo method was used to simulate the dynamics of the exciton cascade starting from initial one-quasiparticle state and taking into account transition rates and particle emission. The consideration was carried out for every ingoing partial angular momentum l_{in} with the weight (2); and for the angular momentum l_{em}, removed by the emitted particle with energy E_{em}, the parametrization was used

$$l_{\mathrm{em}} = 0.5 l_{\mathrm{in}}\sqrt{E_{\mathrm{em}}/E_{\mathrm{in}}}. \quad (15)$$

The memory about initial angular momentum is supposed to be partially conserved. Thus compound nucleus spin distribution at the end of the preequilibrium stage can be calculated. The multiple precompound particle emission was included in consideration. In that case, the neutron and proton spectra emitted in the different stages of the exciton cascade are summed with the weight given by Eq. (4).

$$\frac{dW^i_\pi}{dE_\pi} = \sum_s \frac{dW^{is}_\pi(p_\pi, h_\pi, p_\nu, h_\nu, E_\pi)}{dE_\pi}\tau^{is}(p_\pi, h_\pi, p_\nu, h_\nu), \quad (16)$$

$$\frac{dW^i_\nu}{dE_\nu} = \sum_s \frac{dW^{is}_\nu(p_\pi, h_\pi, p_\nu, h_\nu, E_\nu)}{dE_\nu}\tau^{is}(p_\pi, h_\pi, p_\nu, h_\nu). \quad (17)$$

Here s is used for the cascade stage and i denotes different cascade stories. The precompound spectra are obtained by averaging over all cascade stories.

$$\frac{dW^{\mathrm{prec}}_\pi}{dE_\pi} = \frac{1}{N_{\mathrm{st}}}\sum_i \frac{dW^i_\pi}{dE_\pi}M^i_\pi, \quad (18)$$

$$\frac{dW^{\mathrm{prec}}_\nu}{dE_\nu} = \frac{1}{N_{\mathrm{st}}}\sum_i \frac{dW^i_\nu}{dE_\nu}M^i_\nu, \quad (19)$$

where N_{st} is an exciton cascade story number, and M^i_π, M^i_ν are the proton and neutron multiplicities for one exciton cascade story. The exciton transition cascade is ruptured when one of the following conditions is fulfilled:

(i) Exciton number reaches the limited value $n \geqslant n_{\max}$,
(ii) Particle multiplicity exceeds the limited value $M_\pi \geqslant M_\pi^{\max}$ or $M_\nu \geqslant M_\nu^{\max}$, or
(iii) Total life time of the exciton state exceeds the limit time value $\tau^{is}(p_\pi, h_\pi, p_\nu, h_\nu) \geqslant \tau^{\max}$, which is much less than the statistical life time at given excitation energy. In calculations, the estimation $\tau^{\max} = 0.01\hbar/\Gamma^{\mathrm{stat}}_{\mathrm{tot}}$ and $\tau^{\max} \geqslant 2\times 10^{-22}$s was used. The total particle emission statistical width $\Gamma^{\mathrm{stat}}_{\mathrm{tot}}$ is calculated for the initial energy of the composite nucleus.

After the exciton cascade rupture, the Monte Carlo simulation of story is continued using an equilibrium statistical model to describe the decay of the excited nuclei.

The angular distribution of the neutrons and protons emitted at the precompound reaction stage have been approximated according to the systematics proposed in Ref. [20]. The double differential cross section for preequilibrium particle emission

is described by the expression

$$\frac{d^2\sigma}{d\Omega\, dE} = \frac{1}{4\pi}\frac{d\sigma}{dE}\frac{a}{\sinh(a)}[\cosh(a\cos\theta) + f_{\rm MSD}\sinh(a\cos\theta)], \quad (20)$$

where θ is the emission angle in the center-of-mass frame, $d\sigma/dE$ is the angle-integrated cross section, and $f_{\rm MSD}$ is the fraction of the multistep direct (MSD) contribution in the cross section. The slope parameter a was parametrized as a function of the energy parameter in the exit and entrance channels [20]. According to the general quantum theory for preequilibrium processes [21], the cross section is divided into two parts: statistical MSD and statistical multistep compound (MSC). In the case of only the MSC part contribution at low bombarding energies, the parameter $f_{\rm MSD} = 0$ and the angular distributions are symmetric relative to the polar angle $\theta = 90^\circ$. At higher bombarding energies, particles are supposed to be emitted from purely MSD processes. In the last case, $f_{\rm MSD} = 1$ and the angular distributions have a pronounced peak in the forward direction. The quantum mechanical calculations of the MSD process are quite complex, and only the one-step direct calculations were made at the incident neutron energies below 20 MeV in the ^{238}U(n, f) reaction [13]. Based on the systematics from Ref. [22], one can assume that at the projectile energy above around 25 MeV and emitted particle energy greater than 15 MeV, the emission is purely MSD processes and $f_{\rm MSD} = 1$. At the lower energies, the MSD part decreases approaching to zero at about 5 MeV of the projectile energy.

B. Statistical pre-scission neutron emission

A compound nucleus ensemble with some distributions over mass number $A_{\rm CN}$, charge number $Z_{\rm CN}$, excitation energy $E^{\rm CN}_{\rm ex}$, and spin $J_{\rm CN}$ are formed during the preequilibrium stage. The emission of light particles and γ rays are assumed to start with full statistical decay widths at time $t = 0$ (just after the end of the preequilibrium stage). The stationary fission probability flow over the fission barrier approaches an asymptotic value after a delay time τ_d and the time-dependent fission width is determined by the expression [23,24]

$$\Gamma_f(t) = \Gamma^{\rm BW}_f[1 - \exp(-t/\tau_d)]((1+\gamma^2)^{1/2} - \gamma). \quad (21)$$

Here $\Gamma^{\rm BW}_f$ is statistical Bohr-Wheeler fission width, and γ is a nuclear friction coefficient

$$\gamma = \frac{\beta}{2\omega_b}, \quad (22)$$

where β denotes the reduced dissipation coefficient and ω_b describes the potential curvature at the fission saddle point. The fission delay time parameter was approximated by the formula

$$\tau_d = \ln\left(\frac{10B^{\rm LDM}_f}{T}\right)\left(\frac{1}{2\gamma\omega_{\rm gs}} + \frac{\gamma}{\omega_{\rm gs}}\right), \quad (23)$$

where $B^{\rm LDM}_f$ is a liquid drop model fission barrier, T is the nuclear temperature, and $\omega_{\rm gs}$ stands for the collective frequency at the equilibrium shape. If the fission barrier is too small or temperature is too high when $\frac{10B^{\rm LDM}_f}{T} < 0.1$, then the delay time is negligibly small, $\tau_d = 0$.

The light-particle emission widths for the compound nucleus are calculated according to the expression

$$\Gamma_p\left(E^{\rm CN}_{\rm ex}, J_{\rm CN}\right) = \frac{2s_p+1}{2\pi\rho_{\rm CN}\left(E^{\rm CN}_{\rm ex}, J_{\rm CN}\right)}\sum_{l_p}\sum_{I=|J_{\rm CN}-l_p|}^{I=|J_{\rm CN}+l_p|} \times \int d\varepsilon\rho_d\left(E^{\rm CN}_{\rm ex} - B_p - \varepsilon, I\right)T_{l_p}(\varepsilon). \quad (24)$$

Here s_p and B_p are the spin and binding energy of the particle, $\rho_{\rm CN}$ and ρ_d are level densities of the compound and daughter nuclei, respectively, and $T_{l_p}(\varepsilon)$ are transmission coefficients for particles emitted with angular momentum l_p and kinetic energy ε.

The Bohr-Wheeler width is proportional to the number of the transitional states at the fission barrier

$$\Gamma^{\rm BW}_f\left(E^{\rm CN}_{\rm ex}, J_{\rm CN}\right) = \frac{1}{2\pi\rho_{\rm CN}\left(E^{\rm CN}_{\rm ex}, J_{\rm CN}\right)} \times \int_0^{E^{\rm CN}_{\rm ex}-B_f(J_{\rm CN})}\rho_b\left(E^{\rm CN}_{\rm ex} - B_f(J_{\rm CN}) - \varepsilon, J_{\rm CN}\right)T_f(\varepsilon, J_{\rm CN})\, d\varepsilon, \quad (25)$$

where ρ_b is the level density at the saddle point; transmission coefficients were calculated in the parabolic approximation for a one-humped barrier

$$T_f(\varepsilon, J_{\rm CN}) = \frac{1}{1+\exp\{-2\pi\varepsilon/\hbar\omega_b\}}. \quad (26)$$

The fission barrier of the heated rotating nucleus was calculated using the approximation

$$B_f\left(E^{\rm CN}_{\rm ex}, J_{\rm CN}\right) = C_b B^{\rm LDM}_f\left(E^{\rm CN}_{\rm ex}, J_{\rm CN}\right) - \delta U_{\rm gs}\left(E^{\rm CN}_{\rm ex}\right), \quad (27)$$

where $B^{\rm LDM}_f$ is a liquid drop model fission barrier, C_b is a scale parameter, and $\delta U_{\rm gs}$ is a shell correction at the equilibrium deformation state of a compound nucleus [25]. The liquid drop potential energy of compound nucleus was calculated taking into account the temperature dependence of the surface and Coulomb energies

$$V^{\rm LDM}\left(E^{\rm CN}_{\rm ex}, J_{\rm CN}\right) = E_{\rm surf}(1-\alpha T^2) + E_{\rm Coul}(1-\eta T^2) + \frac{\hbar^2 J_{\rm CN}(J_{\rm CN}+1)}{2\Im_{\rm sph}}B_{\rm rot}. \quad (28)$$

Here $E_{\rm surf}$ and $E_{\rm Coul}$ are the surface and Coulomb energies of the deformed nucleus, respectively, and $\Im_{\rm sph}$ is a rigid-body momentum of inertia of the spherical nucleus. The temperature dependence of the liquid drop energy was introduced within the Tomas-Fermi model [26], and the parameters values $\alpha = 0.012$ MeV^{-2} and $\eta = 0.001$MeV^{-2} have been used. The

rotation function is $B_{\rm rot} = \Im_{\rm sph}/\Im_{\perp}$, where $\Im_{\perp}$ is a rigid-body momentum of inertia associated with the rotation axis perpendicular to the symmetry axis of the deformed nucleus. The inertia momenta were calculated taking into account the diffuseness of the nuclear matter distribution, and the nucleus shape parametrization by Cassinian ovals was used [27].

γ-ray width of the dipole transitions was computed as

$$\Gamma_{\gamma}\left(E_{\rm ex}^{\rm CN}, J_{\rm CN}\right) = \frac{4e^2}{3\pi\hbar{\rm mc}^3}\frac{N_{\rm CN}Z_{\rm CN}}{A_{\rm CN}}\frac{1}{\rho_{\rm CN}\left(E_{\rm ex}^{\rm CN}, J_{\rm CN}\right)} \times \sum_{I=|J_{\rm CN}-1|}^{I=|J_{\rm CN}+1|}\int S_{\gamma}(E_{\gamma})\rho_d\left(E_{\rm ex}^{\rm CN}-E_{\gamma}, I\right)dE_{\gamma}. \quad (29)$$

Here the giant dipole resonance (GDR) strength function for the axially symmetric deformed nucleus has two components

$$S_{\gamma}(E_{\gamma}) = w^{||}\frac{\Gamma^{||}E_{\gamma}^4}{\left(E_{\gamma}^2-E_{\rm GDR}^{||2}\right)^2+\left(\Gamma^{||}E_{\gamma}\right)^2} + w^{\perp}\frac{\Gamma^{\perp}E_{\gamma}^4}{\left(E_{\gamma}^2-E_{\rm GDR}^{\perp 2}\right)^2+\left(\Gamma^{\perp}E_{\gamma}\right)^2}, \quad (30)$$

where $(w^{||}, \Gamma^{||}, E_{\rm GDR}^{||})$ and $(w^{\perp}, \Gamma^{\perp}, E_{\rm GDR}^{\perp})$ stand for weight, width, and position of parallel and perpendicular components of GDR. For the prolate shapes of the heavy nuclei, the GDR parameters were used in accordance with results of Ref. [28].

The change of angular momentum after emission of particles or γ quanta with energy ε was taken into account on average as

$$I^f = I^i - \bar{l}_p(\varepsilon). \quad (31)$$

Here $\bar{l}_p = 1$ for GDR γ quanta and $\bar{l}_p \propto \sqrt{\varepsilon}$ for particles.

The level density of the rotating nucleus at total excitation energy E^* and spin I is calculated in the approximation

$$\rho(E^*, I) = \rho(E^*-E_{\rm rot}, I_{\rm int}), \quad E_{\rm rot} = \frac{\hbar^2}{2\Im_{\perp}}R^2, \quad R^2 = I(I+1)-I_{\rm int}^2, \quad (32)$$

where $I_{\rm int}$ is the internal angular momentum.

After passing the saddle point, the light particles and γ rays are emitted during the saddle-to-scission time, which is altered due to nuclear dissipation [29]

$$\tau_{\rm ssc} = \tau_{\rm ssc}(\gamma=0)[(1+\gamma^2)^{1/2}+\gamma]. \quad (33)$$

In the numerical calculations, the value $\tau_{\rm ssc}(\gamma=0) = 5\times 10^{-21}$ s was used.

The initial excitation energy of the compound nucleus at the saddle-to-scission descent stage is assumed to be an average value of excitation energies at the saddle and scission points, i.e.,

$$E_{sdsc}^{CN}(J_{CN}) = E_{sd}^{CN}(J_{CN}) + 0.5(V_{sd}(J_{CN}) - V_{sc}(J_{CN})). \quad (34)$$

Here E_{sd}^{CN} is the total excitation energy of a compound nucleus just after passing through the fission barrier, and V_{sd} is a potential energy at the saddle point. Potential energy at the scission point $V_{\rm sc}$ is calculated in the framework of the scission point fission model. Momentum of inertia of the composite system at the scission point is

$$\Im_{\perp}^{\rm sc} = \Im_{\perp}^{H} + \Im_{\perp}^{L} + \frac{A(A_{\rm CN}-A)}{A_{\rm CN}}R_{\rm HL}^2, \quad (35)$$

where $\Im_{\perp}^{H}$ and $\Im_{\perp}^{L}$ are momenta of inertia of heavy and light fragments, $R_{\rm HL}$ is a distance between fragments centers, and A is the mass number one of the fragments. At the scission point, the spin of the compound nucleus is divided between the fission fragments and the relative motion degree of freedom according to the relation

$$J_{\rm CN} = I_H + I_L + L, \quad I_H = J_{\rm CN}\frac{\Im_{\perp}^{H}}{\Im_{\perp}^{\rm sc}}, \quad I_L = J_{\rm CN}\frac{\Im_{\perp}^{L}}{\Im_{\perp}^{\rm sc}}. \quad (36)$$

Kinetic energy of the fragments is a sum of the Coulomb interaction energy, kinetic energy at the scission point, and rotational energy,

$$E_{\rm kin} = V_{\rm Coul} + A_{\rm rot}^{\rm rel}L(L+1) + E_{\rm kin}^{\rm sc}, \quad (37)$$

where $A_{\rm rot}^{\rm rel}$ is a rotational constant of a two-fragment system. Kinetic energy of the fragments at scission point consists of two parts,

$$E_{\rm kin}^{\rm sc} = E_{kin\_d}^{\rm sc} + E_{kin\_t}^{\rm sc}, \quad (38)$$

where $E_{kin\_d}^{\rm sc}$ is a dynamical part, which is considered as parameter (it is usually assumed to be $E_{kin\_d}^{\rm sc} = 0$–10 MeV), and a thermal part $E_{kin\_t}^{\rm sc} = 3/2T_{\rm sc}$. A temperature at the scission point, $T_{\rm sc}$ is determined by conditions at the scission point, which will be considered in the next subsection.

The shape and temperature dependences of nuclear friction strength are an important problem in fission dynamics, and at present no definite conclusions can be made about their behavior [1]. It was found that the energy dependence of dissipation strength reveals a threshold character, and the dissipation sets up rather rapidly at a nuclear excitation energy around 40 MeV [30]. In this study, we used the ansatz for the energy dependence of the reduced friction coefficient:

$$\beta(E^*) = \begin{cases} 0 & \text{at} \quad E^* < E_{\rm th}^* \\ \beta_0(1+d_1T+d_2T^2) & \text{at} \quad E^* \geqslant E_{\rm th}^* \end{cases}, \quad (39)$$

where $E_{\rm th}^*$ is the threshold excitation energy value, and β_0, d_1, d_2 are additional parameters describing the temperature dependence of the reduced friction coefficient.

The Monte Carlo simulation method was used to calculate a pre-scission neutron multiplicity and spectra using the compound nuclei parameters formed in the result of the pree-quilibrium neutron and proton emission. The time-dependent statistical approach was applied to the description of particle emission during the fission process up to the scission point to take into consideration the delay time and finite descent time from saddle to scission [31].

C. Post-scission prompt neutron emission

The post-scission neutron multiplicity and spectra are formed as the result of neutron emission from the initial fission fragments which have distributions over mass, kinetic energy, excitation energy, and spin. In the center-of-mass frame of the compound nucleus, the double differential spectra can be presented in the simplified form

$$\frac{d^2M_n^{\rm post}}{dE_n' d\Omega_n'} = \sum_{A_{\rm CN}}\sum_{Z_{\rm CN}}\sum_{A}\int dE_{\rm ex}^{\rm CN} W_{\rm sc}\left(A_{\rm CN}, Z_{\rm CN}, E_{\rm ex}^{\rm CN}\right) \times \iint d\theta_F' d\varphi_F' P(\theta_F', \varphi_F')\frac{M_n^F(A)}{4\pi} \times Y\left(A, A_{\rm CN}, Z_{\rm CN}, E_{\rm ex}^{\rm CN}, \bar{E}_{\rm kin}\right) \times W^F\left(A, E_n^F\right)\sqrt{\frac{E_n'}{E_n^F}}. \quad (40)$$

Here E_n' and E_n^F are neutron energies in the compound nucleus and fission fragment frame, respectively. Fission fragments move with the average total kinetic energy $\bar{E}_{\rm kin}(A)$, and the fragmentation axis direction distributes with probability $P(\theta_F', \varphi_F')$. Neutrons are assumed to be evaporated from the fully accelerated fission fragments and have isotropic angular distribution in the fission fragment frame. The neutron multiplicities $M_n^F(A)$ and spectra $W^F(A, E_n^F)$ depend mainly on the initial fragment excitation energy. Contributions from different fission fragments with the corresponding yields $Y(A)$ for the compound nucleus ensemble $W_{\rm sc}(A_{\rm CN}, Z_{\rm CN}, E_{\rm ex}^{\rm CN})$ at the scission point are summed. For adequate description of the post-scission neutron multiplicities and spectra, the excitation energy, kinetic energy, and mass distributions of the primary fission fragments have to be calculated in the wide excitation energy region of different compound nuclei.

The mean kinetic and excitation energies of fragments have been calculated in the framework of the fission scission point model. The scission point configuration is approximated by two nascent spheroidal-shaped fragments with a distance between the tips of the fragments $\Delta_{\rm tip} = 2$–3 fm. Full calculations of the properties of scission point configuration using the macroscopic-microscopic approach are too time consuming. In practical calculations, we used the simple version of the model.

Potential energy at the scission point consists of the Coulomb interaction energy between fragments and the deformation energy of both fragments, that is,

$$V_{\rm sc} = V_{\rm sc}^{\rm Coul} + E_{\rm def}^L + E_{\rm def}^H, \quad (41)$$

where $V_{\rm sc}^{\rm Coul}$ is the Coulomb energy, and $E_{\rm def}^L$ and $E_{\rm def}^H$ are deformation energies of ellipsoidal fragments. Deformation energy was computed in the parabolic approach with

$$E_{\rm def} = C_d(b - R_0)^2, \quad R_0 = r_0 A^{1/3}, \quad r_0 = 1.35\,{\rm fm}, \quad (42)$$

where b is the large semi-axis of a deformed fragment. The stiffness coefficient C_d depends on the shell correction δU and temperature according to the formula

$$C_d = C_d^{\rm LDM}\frac{K - \delta U}{K + \delta U}, \quad K = 8\,{\rm MeV}. \quad (43)$$

The temperature dependence of the shell corrections was described as

$$\delta U(T) = \delta U(0)\frac{2}{1 + \exp(t)}, \quad t = T\frac{2\pi^2}{41A^{-1/3}}. \quad (44)$$

The stiffness coefficient in the liquid drop model approximation is equal to

$$C_d^{\rm LDM} = \frac{0.16\pi}{r_0^2}\left[a_2\left(1 - k_s\frac{(N-Z)^2}{A^2}\right) - \frac{1}{2}c_3\frac{Z^2}{A}\right], \quad (45)$$

where $a_2 = 18.56$ MeV, $k_s = 1.79$, and $c_3 = 0.717$ MeV.

The temperature at the scission point is determined from the energy balance

$$Q_f(A_{\rm CN}, Z_{\rm CN}, A, Z) + E_{\rm ex}^{\rm CN} = V_{\rm sc} + E_{\rm sc}^* + E_{\rm kin}^{\rm sc} + A_{\rm rot}^{\rm rel}L(L+1). \quad (46)$$

Here $Q_f(A_{\rm CN}, Z_{\rm CN}, A, Z)$ is the fission Q value, and the relative angular momentum is defined from expressions (36). Thermal energy $E_{\rm sc}^*$ is divided between fragments according to the thermal equilibrium condition

$$\frac{E_{\rm sc}^{*H}}{E_{\rm sc}^{*L}} = \frac{a^H}{a^L}, \quad (47)$$

with the level density parameters $a^{L(H)}$. Fragment average kinetic energy, which is a sum of the Coulomb interaction energy, the scission kinetic energy, and rotation energy [see Eq. (37)], was calculated at the minimum of the potential energy at the scission point. Average excitation energy of the primary fragment is a sum of energy deformation and thermal energy and was also calculated at the minimum of the potential energy at the scission point.

Shell structure of the fission fragment at the scission point plays a decisive role in the fragment mass dependence of the mean neutron multiplicity $M_n^F(A)$ and its temperature dependence [32]. Effects of that shell structure have been taken into account by determining the shell corrections $\delta U(A)$ for reference compound nuclei ^{236}U and ^{252}Cf using experimental data of average neutron multiplicities in the spontaneous fission of ^{252}Cf and thermal neutron induced fission of ^{235}U. The linear interpolation or extrapolation procedure to the compound nucleus mass numbers between these reference shell correction curves $\delta U(A)$ were used to obtain the shell correction of fragments at scission point in the fission of other compound nuclei. The neutron multiplicities $M_n^F(A)$ and spectra $W^F(A, E_n^F)$ at the most probable fragment charge were calculated within the standard statistical model. The parameters of the GDR strength function for the spherical heated fragments were taken from Ref. [28]. The multimodal approach in the nuclear fission was used to describe the primary fragment mass distribution $Y(A, A_{\rm CN}, Z_{\rm CN}, E_{\rm ex}^{\rm CN})$ for compound nuclei from Ra to Cf and excitation energies up to 100 MeV [33,34].

III. RESULTS AND DISCUSSION

The model described in the previous section has been tested using available experimental data on the prompt fission neutron characteristics in the proton and neutron induced fission of heavy nuclei. Contribution of the preequilibrium particle emission depends strongly on the residual interaction matrix element M^2. The amount of energy removed by particles emitted at the precompound stage influences the particle evaporation during the fission process. In that study, the residual interaction matrix element and its energy dependence were taken in the form (8) as proposed in Ref. [18]. The level densities of the compound nuclei were calculated according to the systematics of Ref. [35].

The most valuable information about the prompt fission neutron emission mechanism at intermediate energies can be obtained from the double differential fission neutron spectra. But besides limited information on the ^{242}Pu (p, f) reaction at $E_p = 13, 20$, and 55 MeV [6], there is no experimental data at the intermediate energies. In that work, the neutron spectra were obtained in coincidence with fission fragments measured around the angle $\theta_F \approx 88^\circ$ relative to beam direction. The comparison between experimental neutron spectra at angles in the laboratory frame $\Theta_n = 18^\circ$, and 107° (points with error bars) and theoretical ones (open circles) in the ^{242}Pu (p, f) reaction at $E_p = 20$ MeV is shown in Fig. 1. The calculated preequilibrium (dashed line), pre-scission (dotted line), and post-scission (solid line) components are also presented in that figure. At that incident proton energy, the post-scission neutrons give the main contribution in neutron yield. In the direction perpendicular to the proton beam direction and close to the fission axes direction ($\Theta_n = 107^\circ$), the preequilibrium

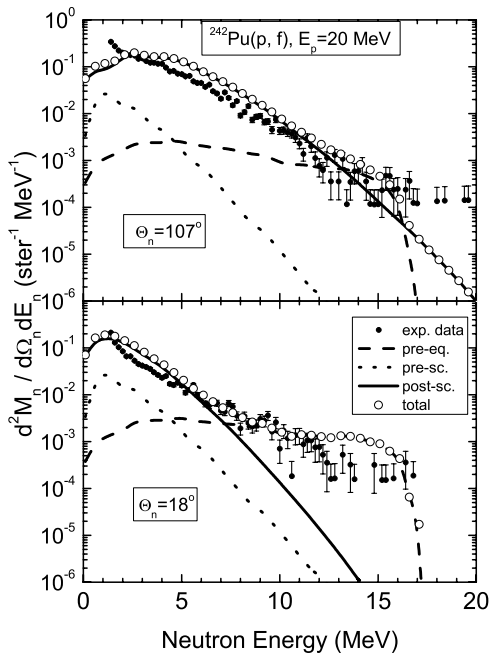

FIG. 1. Experimental (points with error bars) and theoretical (circles) fission prompt neutron spectra in ^{242}Pu (p, f) at $E_p = 20$ MeV at laboratory frame angles 18° and 107° in coincidence with the fission fragment detectors placed at the angle around 88°.

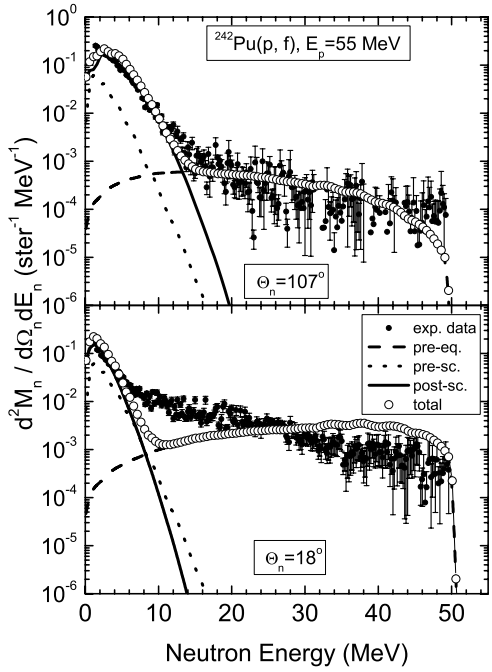

FIG. 2. Same as Fig. 1, but for $E_p = 55$ MeV.

mechanism may be detected as a bump near the statistical limit of the neutron spectrum. In the forward direction, one can clearly see a high neutron energy tail upon the evaporation neutron spectrum.

Contributions from different neutron emission mechanisms and comparison between experimental spectra and theoretical ones for the same reaction at $E_p = 55$ MeV are presented in Fig. 2. At that incident proton energy, the preequilibrium high neutron energy spectrum tail becomes important at all angles and increases substantially the average fission neutron energy. The proposed model gives a satisfactory description of the available experimental double differential fission neutron spectra. Additional measurements are needed to understand the discrepancies between experimental spectra at $\Theta_n = 18^\circ$ in the neutron energy interval 10–20 MeV (see Fig. 2).

Precompound proton emission in the nucleon induced fission of heavy nuclei becomes important at an incident energy higher than 20 MeV. The dependencies of the preequilibrium neutron and proton multiplicities on the projectile energy calculated in the neutron and proton induced fission of ^{238}U are presented in Fig. 3. In the case of the proton projectile, the proton preequilibrium emission is about two times more intense than that in the neutron induced fission because of the different nucleon composition of the initial exciton states. The smooth irregularity in the incident energy dependence of preequilibrium neutron multiplicity $M_n^{\text{pre-eq}}$ near 40 MeV can be explained by the preequilibrium proton emission competition.

Pre-scission neutron spectrum and multiplicity are defined by the excitation energy of the compound nucleus after preequilibrium particle emission and by the competition between particle evaporation and fission channels which depends strongly on the strength of the nuclear friction. Theoretical calculations of pre-scission, post-scission, and total neutron

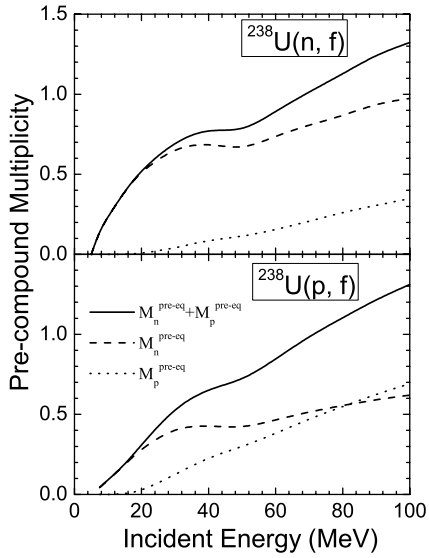

FIG. 3. Calculated incident energy dependences of neutron (dashed lines) and proton (dotted lines) precompound emission multiplicities in ^{238}U(n, f) and ^{238}U(p, f) reactions.

multiplicities in the proton induced fission of ^{238}U are shown in Fig. 4, together with experimental data [4,5]. Calculations were carried out with the following parameters in Eq. (39): $\beta_0 = 2.5 \times 10^{21}\ s^{-1}$, $E^*_{\rm th} = 20$ MeV, $d_1 = 6\ {\rm MeV}^{-1}$, and $d_2 = 2\ {\rm MeV}^{-2}$. Satisfactory description of the experimental dependence of the pre-scission neutron multiplicity was achieved; therefore, one can rely on the parameters describing friction effects. The model predicts a saturation of $M_n^{\rm pre-sc}(E_p)$ dependence at proton energies higher than 60 MeV, because the preequilibrium particles remove a substantial part of the initial total excitation energy. Proton energy dependence of the post-scission neutron multiplicity $M_n^{\rm post}(E_p)$ saturates at $E_p > E^*_{\rm th}$. There are only two experimental points at $E_p = 50$ and 60 MeV with almost equal $M_n^{\rm post}$ values which are larger than the calculated ones. Experimental total neutron multiplicity at $E_p = 60$ MeV exceeds the predicted value substantially, which may indicate possible unaccounted-for systematic uncertainties in the data processing.

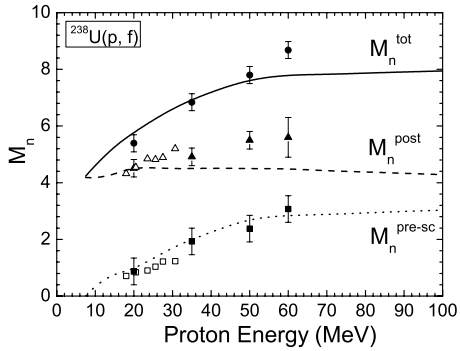

FIG. 4. Experimental (points) and theoretical (lines) pre-scission, post-scission, and total neutron multiplicities in ^{238}U(p, f) reaction as function of proton energy. Open points are from M. Strecker *et al.* [4] and solid points are from Rubchenya *et al.* [5].

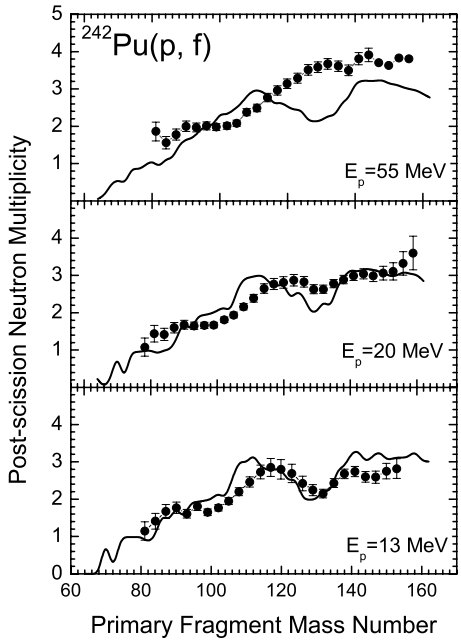

FIG. 5. Experimental (points) [6] and theoretical (lines) post-scission neutron multiplicities in ^{242}Pu(p, f) reaction as function of primary fragment mass at $E_p = 13$, 20, and 55 MeV.

Fission fragment mass dependence of the post-scission neutron multiplicity gives information on the potential energy surface structure and temperature near the scission point and on the attenuation of the shell effects with increasing excitation energy. In Fig. 5, the experimental [6] and calculated post-scission neutron multiplicities in ^{242}Pu(p, f) are compared for proton incident energies 13, 20, and 55 MeV. The theoretical model describes relatively well the experimental dependencies at the two lowest proton energies. At these energies, the minimum near $A = 132$, connected with nuclear shells $Z = 50$ and $N = 82$, is still visible. But there is unexpected disagreement between measured and predicted $M_n^F(A)$ values in the interval $A = 120-140$ at $E_p = 55$ MeV, where theoretical dependence has a minimum. According to the model described in previous sections, the temperature near scission practically saturates at incident proton or neutron energy above 30 MeV, and therefore shell effects are not smeared out totally. That conclusion can

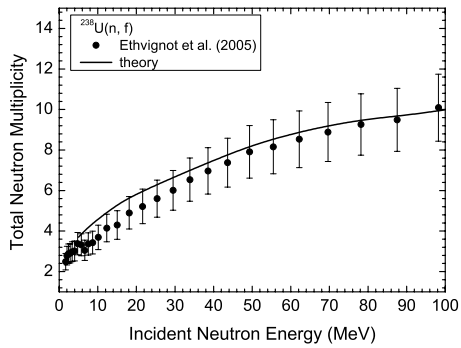

FIG. 6. Experimental (points) [36] and theoretical (line) total prompt fission neutron multiplicity in ^{238}U(n, f) reaction as function of incident neutron energy.

be proved by measurement of the $M_n^F(A)$ dependences in the ^{238}U (p, f) reaction at $E_p = 20, 35, 50$, and 60 MeV [5].

The comparison of the model calculations against the new experimental data for the prompt fission neutron multiplicity in the neutron induced fission of ^{238}U [36] is shown in Fig. 6. The model describes well the $M_n(E_n)$ dependence at intermediate energy. In the present study, fission cross section at low energies was calculated without including two humped fission barrier properties; therefore, the structure in the $M_n(E_n)$ dependence is not well described.

IV. CONCLUSION

In conclusion, the new theoretical model for describing the fission prompt neutron spectra and multiplicity in proton and neutron induced fission was formulated and analyzed. precompound nucleon emission was described in the framework of the two-component exciton model using a Monte Carlo method, which allows one to incorporate a time duration criterion for the preequilibrium stage of reaction. Decay of the excited compound nuclei, formed after the preequilibrium neutron and proton emission, was treated within a time-dependent statistical model with inclusion of the main dynamical effects of nuclear friction on the fission width and saddle-to-scission descent time. It was shown that the saturation in the incident energy dependence of the pre-scission neutron multiplicity can be explained by the preequilibrium particle emission and by the nuclear friction effects.

Particle emission at the precompound stage and during evolution to scission determines the composition, excitation energy, and angular momentum of the compound system before its division into fragments. To calculate the primary fission fragment excitation and kinetic energies, the scission point fission model with the semiphenomenological shell corrections and its temperature dependence was used. The post-scission neutron spectra and multiplicity from the individual primary fission fragment at the average excitation and kinetic energies were calculated within the standard statistical approach. The fragment mass integrated neutron characteristics were obtained using calculated fragment mass distribution. The model described consistently the prompt fission neutron characteristics and fission cross section.

Double differential spectra thus calculated were compared with the experimental data in the proton induced fission of ^{242}Pu at incident energies of 20 and 55 MeV, measured in coincidence with the fission fragments. The data were well reproduced by the present calculation method, and the different emission mechanism contributions were extracted. The statistical pre-scission, post-scission, and total neutron multiplicities predicted by the present model are close to the experimental data in the proton induced fission of ^{238}U up to an incident energy of 60 MeV. The present model consistently takes into account the precompound particle emission and nuclear friction effects in the fission process and predicts the saturation in the energy dependence of $M_n^{\mathrm{pre-sc}}$ above 50 MeV and the post-scission multiplicity above the threshold in the temperature dependence of the reduced friction coefficient [see Eq. (39)]. However, the two experimental values of M_n^{post} at $E_p = 50$ and 60 MeV are underestimated, and additional experimental data are needed to understand that disagreement. Precompound prompt fission neutron and proton multiplicities were calculated as function of the projectile incident energy, and it was found that the proton preequilibrium emission in the proton induced fission is more intensive than that in the neutron induced fission because the initial exciton states are different in each case.

The calculations of the post-scission neutron multiplicity for individual fission fragments were carried out and compared with the experimental data in the proton-induced fission of ^{242}Pu at $E_p = 13, 20$, and 55 MeV [6]. The present model describes well the $M_n^F(A)$ dependences at two lower incident energies, but there is disagreement with the 55 MeV data, where the calculations underestimate the neutron multiplicities in the fragment mass interval 120–140. It was found that the average excitation energy of the fragment pair almost reaches saturation at the incident nucleon energy above 30–40 MeV because of the increasing amount of energy removed by particle emission before scission, and the shell structure effects are not totally washed out. Prompt fission neutron total multiplicity was described well by the present calculations in the neutron-induced fission of ^{238}U up to a neutron energy of 100 MeV. The present calculation method can be generalized to the low incident energies by including the fission barrier structure. The present model provides a theoretical tool for experimental data analysis and practically important relevant nuclear data predictions.

ACKNOWLEDGMENTS

I thank Prof. J. Äystö for his enthusiastic support and fruitful discussions. This work was supported by the Finnish Center of Excellence Programme 2000–2005 (Project No. 44875, Nuclear and Condensed Matter Physics Programme at JYFL) and the Finnish Center of Excellence Programme 2006–2011 (Project No. 213503, Nuclear and Accelerator Base Physics Programme at JYFL). I also acknowledge the financial support of the European Community under the FP6 "Research Infrastructure Action–Structuring the European Research Area" EURISOL DS Project Contract No. 515768 RIDS.

[1] D. Hilscher and H. Rossner, Ann. Phys. Fr. **17**, 471 (1992).
[2] E. Cheifetz, Z. Fraenkel, J. Galin, M. Lefort, J. Péter, and X. Tarrago, Phys. Rev. C **2**, 256 (1970).
[3] Z. Fraenkel, I. Mayk, J. P. Unik, A. J. Gorski, and W. D. Loveland, Phys. Rev. C **12**, 1809 (1975).
[4] M. Strecker, R. Wien, P. Plischke, and W. Scobel, Phys. Rev. C **41**, 2172 (1990).
[5] V. A. Rubchenya, W. H. Trzaska, D. N. Vakhtin, J. Äystö, P. Dendooven, S. Hankonen, A. Jokinen, Z. Radivojevich, J. C. Wang, I. D. Alkhazov, A. V. Evsenin, S. V. Khlebnikov, A. V. Kuznetsov, V. G. Lyapin, O. I. Osetrov, G. P. Tiourin,

and Yu. E. Penionzhkevich, Nucl. Instrum. Methods Phys. Res., Sect. A **463**, 653 (2001).
[6] V. A. Rubchenya, W. H. Trzaska, I. M. Itkis, M. G. Itkis, J. Kliman, G. N. Kniajeva, N. A. Kondratiev, E. M. Kozulin, L. Krupa, I. V. Pokrovski, V. M. Voskressenski, F. Hanappe, T. Materna, O. Dorvaux, L. Stuttge, G. Chubarian, S. V. Khlebnikov, D. N. Vakhtin, and V. G. Lyapin, Nucl. Phys. **A734**, 253 (2004).
[7] B. E. Watt, Phys. Rev. **87**, 1037 (1952).
[8] J. C. Browne and F. S. Dietrich, Phys. Rev. C **10**, 2545 (1974).
[9] D. G. Madland and J. R. Nix, Nucl. Sci. Eng. **81**, 213 (1982).
[10] H. Märten and D. Seeliger, J. Phys. G **10**, 349 (1984).
[11] B. F. Gerasimenko and V. A. Rubchenya, At. Energ. **59**, 335 (1985).
[12] F.-J. Hambsch, S. Oberstedt, G. Vladuca, and A. Tudora, Nucl. Phys. **A709**, 85 (2002).
[13] T. Kawano, T. Ohsawa, M. Baba, and T. Nakagava, Phys. Rev. C **63**, 034601 (2001).
[14] V. M. Maslov, Yu.V. Porodzinskij, M. Baba, A. Hasegava, N. Kornilov, A. B. Kagalenko, and N. A. Tetereva, Eur. Phys. J. A **18**, 93 (2003).
[15] V. M. Maslov, Yu. V. Porodzinskij, M. Baba, A. Hasegava, N. Kornilov, A. B. Kagalenko, and N. A. Tetereva, Phys. Rev. C **69**, 034607 (2004).
[16] A. Tudora, G. Vladuca, and B. Morillon, Nucl. Phys. **A740**, 33 (2004).
[17] E. Gadioli and P. E. Hodgson, *Pre-equilibrium Nuclear Reaction* (Clarendon Press, Oxford, 1992).
[18] A. J. Koning and M. C. Duijvestijn, Nucl. Phys. **A744**, 15 (2004).
[19] F. Rejmund, A. V. Ignatyuk, A. R. Junghans, and K.-H. Schmidt, Nucl. Phys. **A678**, 215 (2000).
[20] C. Kalbach, Phys. Rev. C **37**, 2350 (1988).
[21] H. Feshbach, A. Kerman, and S. Koonin, Ann. Phys. (NY) **125**, 429 (1980).
[22] C. Kalbach and F. M. Mann, Phys. Rev. C **23**, 112 (1981).
[23] H. A. Kramers, Physika **7**, 284 (1940).
[24] P. Grangé, S. Hassani, H. A Weidenmüller, A. Gavron, J. R. Nix, and A. J. Sierk, Phys. Rev. C **34**, 209 (1986).
[25] W. D. Myers and W. J. Swiatecki, Nucl. Phys. **A81**, 1 (1966).
[26] X. Campi and S. Stringari, Z. Phys. A **309**, 239 (1983).
[27] V. V. Pashkevich, Nucl. Phys. **A169**, 275 (1971).
[28] M. Thoennessen, D. R. Chakrabarty, M. G. Herman, R. Butsch, and P. Paul, Phys. Rev. Lett. **59**, 2860 (1987).
[29] H. Hofman and J. R. Nix, Phys. Lett. **B122**, 117 (1983).
[30] P. Paul and M. Thoennessen, Annu. Rev. Nucl. Part. Sci. **44**, 65 (1994).
[31] V. A. Rubchenya, A. V. Kuznetsov, W. W. Trzaska, D. N. Vakhtin, A. A. Alexandrov, J. Äystö, S. V. Khlebnikov, V. G. Lyapin, O. I. Osetrov, Yu. E. Penionzhkevich, Yu. V. Pyatkov, and G. P. Tiourin, Phys. Rev. C **58**, 1587 (1998).
[32] R. Vandenbosch and J. R. Huisenga, *Nuclear Fission* (Aademic Press, New York and London, 1973).
[33] V. A. Rubchenya and J. Äystö, Nucl. Phys. **A701**, 127c (2002).
[34] I. Tsekhanovich, N. Varapai, V. Rubchenya, D. Rochman, G. S. Simpson, V. Sokolov, and I. Al Mahamid, Phys. Rev. C **70**, 044610 (2004).
[35] A. V. Ignatyuk, G. N. Smirenkin, and A. S. Tishin, Sov. J. Nucl. Phys. **21**, 255 (1975).
[36] T. Ethvignot, M, Delvin, H. Duarte, T. Granier, R. C. Haight, B. Morillon, R. O. Nelson, J. M. O'Donnell, and D. Rochman, Phys. Rev. Lett. **94**, 052701 (2005).